Journal of Applied Polymer Science

Ultrathin buffer layer at organic/organic interface for managing the recombination profile in organic light-emitting diodes: Metal versus dielectric buffer

Davood Kalhor,[1] Ezeddin Mohajerani,[1] Omid HashemiPour,[2] Akram SalehiKian,[1] Mohsen Shojaeifar,[1] Mohammad Rasoul Babaei[1]

[1]Laser and Plasma Research Institute, Shahid Beheshti University, G.C., Tehran 1983963113, Iran

[2]Department of Electrical and Computer Engineering, Shahid Beheshti University, G.C., Tehran 1983963113, Iran

Correspondence to: E. Mohajerani (E-mail: e-mohajerani@sbu.ac.ir)

ABSTRACT: We report on the utilization of an ultrathin buffer layer at the organic/organic (O/O) interface to enhance device efficiency in organic light-emitting diodes. Two different kinds of buffer layers are examined: metal and dielectric. It is shown that employment of an ultrathin Ag layer with a thickness of 1–2 nm enhances the device performance, while a MgF_2 dielectric buffer cannot affect the device properties considerably. In particular, the turn-on voltage of the device with an appropriate buffer layer is reduced about 3 V, its current efficiency increases by a factor of more than three, and the power efficiency increases by a factor of more than five in comparison to the control device when a Ag buffer layer is introduced at the O/O interface. By employment of the buffer layer at the interface, an accumulation of current carriers appears within the device that redistribute the recombination profile toward the interior part of the emissive layer. Also, morphological examinations reveal that distinguishable phase segregation occurs in the blend of the hole-transport layer. In particular, the polymer component remains at the surface and facilitates the hole transport into the successive layers. © 2016 Wiley Periodicals, Inc. J. Appl. Polym. Sci. **2016**, *133*, 43894.

KEYWORDS: dielectric properties; optical properties; properties and characterization; structure-property relations; surfaces and interfaces

Received 10 February 2016; accepted 4 May 2016

DOI: 10.1002/app.43894

INTRODUCTION

Organic light-emitting diodes (OLEDs) have been a topic of special interest in many research studies owing to their potential advantages over competing technologies such as fluorescent lamps and liquid crystal displays.[1–5] The establishment of balanced electrons and holes in OLEDs results in improved electrical and optical properties and therefore superior device efficiency.[1,4] Optimizing the electrical characteristics in OLEDs also leads to an enhancement in device lifetime.[3–5]

It has been demonstrated that employment of ultrathin buffer layers at a metal/organic interface can considerably improve carrier injection into the device. Tang and coworkers showed[6–8] that a thin layer of LiF can be inserted at the cathode/organic interface to enhance the device performance. Buffer layers such as MgF_2, CaF_2, MgO, Al_2O_3, and NaCl have been shown to be effective in enhancing the electrical characteristics of OLEDs.[9–14] For instance, Chen *et al.*[15] revealed that an ultrathin MgF_2 layer can act as both electron-injection layer at the cathode/organic interface and as a hole-blocking layer at the anode/organic interface. Recently, the application of metal buffers such as indium has been presented to enhance device properties.[16] Also, many studies have been conducted[17–23] in order to understand the physics of carrier transfer at the metal/organic interface in an OLED structure.

Despite many investigations concerning the utilization of buffer layers to treat the cathode/organic and anode/organic interfaces, a highly paramount and effective interface in the device structure, that is, the organic/organic (O/O) interface, has been barely considered in the literature. The organic/organic interface has an extreme impact on device performance because the exciton formation and recombination area is mostly established at or near the interface where the light emission takes place. At the same time, employment of metals as buffer layers has rarely been investigated in OLED structures.

In the present paper, we demonstrate the utilization of an ultrathin buffer layer (BL) at the organic/organic interface. It is observed that insertion of an appropriate buffer layer at the interface improves the device performance considerably.

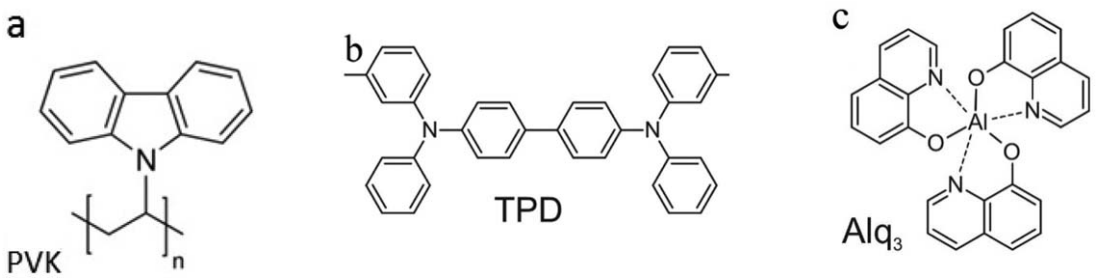

Figure 1. Molecular structures of the organic materials present at the organic/organic interface: (a) poly(vinyl carbazole) (PVK), small molecule semiconductor, (b) *N,N′*-bis(phenyl)benzidine (TPD), and (c) tris(8-hydroxyquinolinato)aluminum (Alq_3).

Dielectric buffer and metal buffer layers are examined (MgF_2 versus Ag), and their effectiveness is compared. In particular, we demonstrate that, by employing an ultrathin layer of Ag with a thickness of 1–2 nm at the O/O interface, the turn-on voltage of the device is reduced, the current efficiency increases, and the power efficiency increases in comparison to the control device without any buffer layer. Also, the rational origin of the performance improvement is inspected. The investigations reveal that utilization of an ultrathin Ag buffer not only affects the morphology of the organic/organic interface but also redistributes the recombination profile.

EXPERIMENTAL

Materials

For the hole-transport layer (HTL), a mixture of *N,N′*-bis(phenyl)benzidine (TPD) small molecule semiconductor and poly(vinyl carbazole) (PVK) polymer with a ratio of 3:2 was employed. The mixture presents superior properties compared to the individual materials. For the emissive layer, tris(8-hydroxyquinolinato)aluminum (Alq_3) was exploited. Alq_3 serves as an electron-transport layer as well. Figure 1 shows the molecular structures of the materials that are present at the organic/organic interface. Indium tin oxide (ITO)–coated substrates were exploited as the anode electrode. Also, a poly(3,4-ethylenedioxythiophene):poly(styrene sulfonate) (PEDOT:PSS) layer was deposited as a hole-injection layer. On the other side, silver (Ag) and aluminum (Al) were used as the metal cathode electrode. Indeed, an ultrathin layer of Ag (metal buffer) or MgF_2 (dielectric buffer) was inserted at the organic/organic interface adjoining the recombination zone. All of the chemicals, except the ITO substrates, were purchased from Sigma-Aldrich (China) or Merck (Germany) and used without any further purification. ITO-coated substrates were purchased from Diamond Coating (UK). The ITO coating possesses a sheet resistance, a layer thickness, and a work function of 20 Ω/Sq, 150 nm, and 5.2 eV, respectively. The schematic of the basic device structure is shown in Figure 2.

Device Fabrication

ITO-coated substrates were patterned to fit with a metal shadow mask prior to any other preparation process. Then, the samples were cleaned in acetone and isopropyl alcohol baths and dried with a nitrogen stream. PEDOT:PSS was deposited on the top of the substrates by using a spin-coating system and backed at 120 °C for 20 min. The thickness of the polymer layer was ~100 nm. Next, the solution of TPD and PVK (3:2) was prepared in chloroform as the common solvent, and subsequently the solution was spin-coated and backed at 90 °C for 20 min to form the first organic layer with a thickness of ~100 nm. This layer operates as the hole-

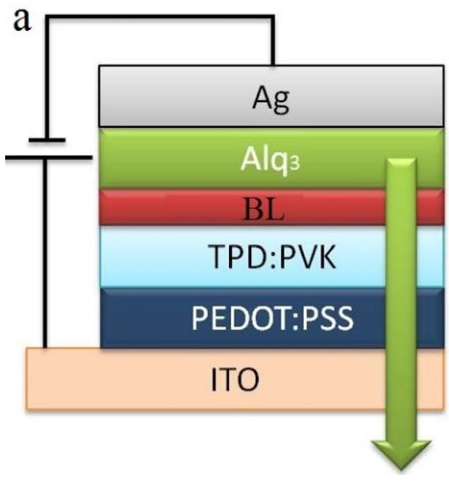

Figure 2. The schematic of the device structure and the ultrathin buffer layer at the organic/organic interface. [Color figure can be viewed in the online issue, which is available at wileyonlinelibrary.com.]

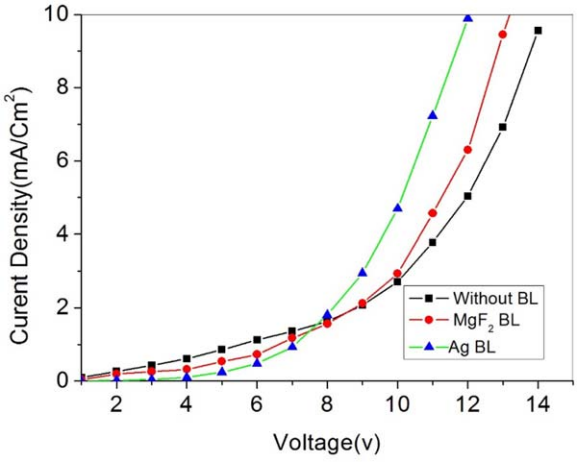

Figure 3. Current density versus voltage for the devices: squares: without any buffer; circles: with MgF_2 (1 nm); and triangles: with Ag (1 nm) buffer layer. [Color figure can be viewed in the online issue, which is available at wileyonlinelibrary.com.]

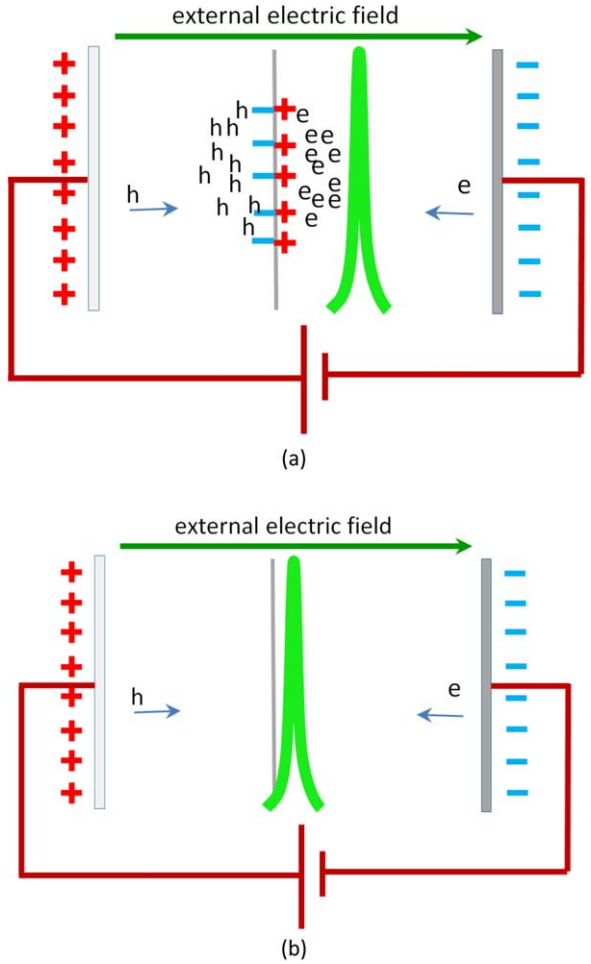

Figure 4. Schematic operation of (a) the device employing a Ag buffer layer, and (b) the control device without a buffer layer. The accumulation of the current carriers at the O/O interface owing to the presence of the Ag buffer layer rearranges the recombination profile. [Color figure can be viewed in the online issue, which is available at wileyonlinelibrary.com.]

transport layer and electron-blocking layer (EBL).[24] The samples were then transferred to the high-vacuum coating system inside a glove box for physical vapor deposition (PVD). In the vacuum chamber, first, an ultrathin layer of Ag metal or MgF_2 dielectric was thermally deposited, and then the deposition of the second organic layer, that is, Alq_3 as the emissive layer (EML) and electron-transport layer, was performed. Finally, the cathode electrode was thermally deposited, Ag or Al, with a thickness of 80 nm at an operating pressure of $<8 \times 10^{-6}$ mbar. The active area of the devices was around 4×5.5 mm^2. It is noteworthy that all deposition processes were performed under precisely controlled conditions in order to minimize any undesired effects on the morphology of the organic layers. In particular, the distance between the samples and the evaporation sources was designed to be as long as 25 cm, the deposition rate was kept as low as 0.1 Å/S, and a sample holder with capacity of 16 devices was exploited for the deposition of the Ag metal and MgF_2 dielectric layer. Also, the cathode deposition was performed in two steps. The deposition rate was kept as low as 0.2 Å/S at the beginning of the evaporation, ~20 nm, in order to prevent any damage to the underlying organic layers, and then the evaporation rate was increased to 0.6 Å/S.

Measurements

A Sigma Instruments SQ160 crystal thickness monitor and a DekTak (Germany) 8000 profilometer were used as thickness-measurement systems. A Keithley (Korea) source meter, model 2400, was utilized to obtain current–voltage characteristics. Also, USB2000 and HR4000 Ocean Optics (USA, Florida) spectrometers were employed to record the Electroluminescence (EL) and Photoluminescence (PL) of the fabricated OLEDs. A Lutron YK2005LX light meter was used to measure the light intensity, and the surface morphology of the samples was captured by atomic force microscopy (AFM) images, which were acquired with a DME (Danish Micro Engineering (Denmark)) DualScope DS 95.

RESULTS AND DISCUSSION

Figure 3 compares the current density against voltage characteristics of the devices with a Ag cathode electrode without any buffer, with 1 nm MgF_2 buffer, and with 1 nm Ag buffer layers. As can be seen, the J–V characteristic of the device almost remains unchanged and is affected only slightly by the insertion of the buffer layer for both the metal and dielectric buffer layers. Principally, the current carriers can directly tunnel through the ultrathin buffer because the energy barrier is extremely narrow. Nevertheless, the slight decrease in the J–V characteristics can be associated with the accumulation of the current carriers close to the buffer layer, as schematically depicted in Figure 4(a). First, the external electric field induced a dipole moment in the buffer layer. This local dipole attracts and accumulates the free current carriers, and consequently a net internal electric field is established opposite to the external field that slightly decreases the total current density. It should also be emphasized that formation of the dipole moments and the accumulation of the current carriers are more prominent when the Ag ultrathin layer is utilized than when a dielectric layer is employed. It might be postulated that MgF_2 as a dielectric possesses natural atomic dipoles that are oriented randomly

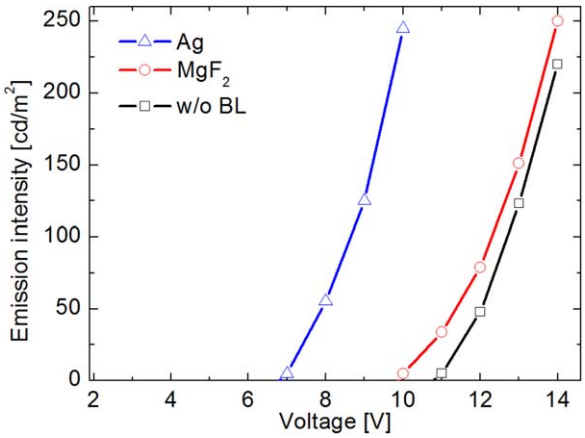

Figure 5. Emission intensity against voltage for the device without any buffer and the devices with MgF_2 (1 nm) and Ag (1 nm) buffer layers. [Color figure can be viewed in the online issue, which is available at wileyonlinelibrary.com.]

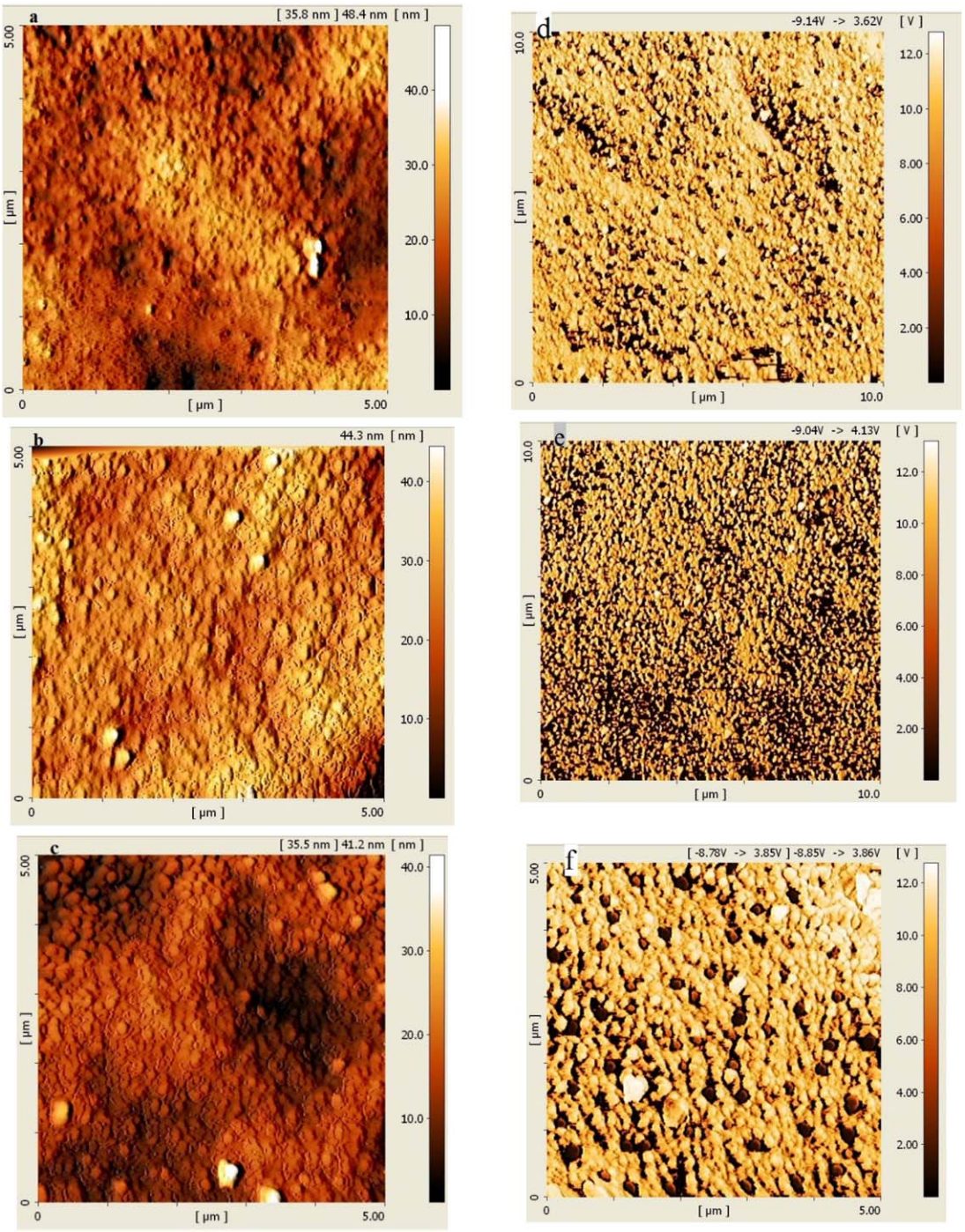

Figure 6. Atomic force microscope microstructure images of glass/ITO/PEDOT:PSS/PVK:TPD/BL surface: (a) height trace for sample without buffer, (b) height trace for sample with 1 nm Ag BL, (c) height trace for sample with 1 nm MgF_2 BL, (d) phase trace for sample without buffer, (e) phase trace for sample with 1 nm Ag BL, and (f) phase trace for sample with 1 nm MgF_2 BL. [Color figure can be viewed in the online issue, which is available at wileyonlinelibrary.com.]

at the organic/organic interface during the layer deposition. The randomness in the direction of the natural atomic dipole for the dielectric buffer layer attenuates the accumulation of current carriers close to the interface.

Next, Figure 5 demonstrates the light-emission intensity versus voltage (L–V) characteristics of the fabricated devices. As can be observed, the L–V characteristic of the device is enhanced surprisingly in particular when the Ag buffer layer is inserted into the device structure. It might be argued that the deposition of the ultrathin metal buffer layer manages the exciton formation and exciton annihilation at the organic/organic interface and consequently improves the device performance. Two phenomena might be considered as the origin of the performance enhancement, namely, morphological

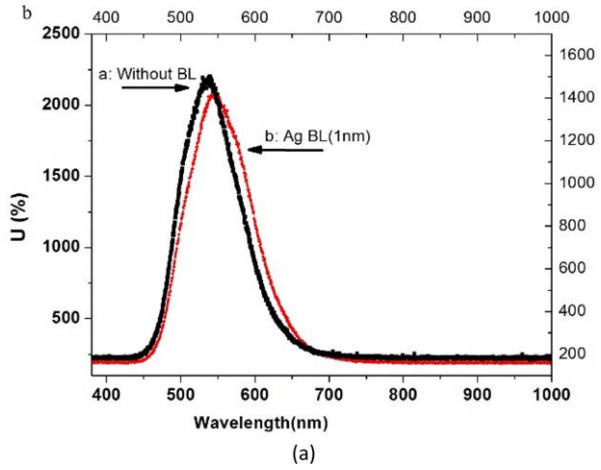

Figure 7. EL spectra for the control device without BL and the device with 1 nm Ag BL. [Color figure can be viewed in the online issue, which is available at wileyonlinelibrary.com.]

treatment of the surface at the interface and then redistribution of the recombination zone.

Figure 6 reveals the AFM tapping-mode and phase-mode images of the surface of the interface, glass/ITO/PEDOT:PSS/PVK:TPD/BL, for the samples without buffer [(a) and (d)], with Ag buffer [(b) and (e)], and with MgF_2 buffer [(e) and (f)]. The tapping-mode images present well-distinguishable submicron regions appearing at the surface of the interface after deposition of the Ag and MgF_2 buffer layers. These areas can be interpreted as good segregation of the blend components, that is, PVK polymer, which remains at the surface. Similarly, the homogenous phase contrast in phase-mode images confirms that the polymer component (PVK) alone dominates at the surface of the interface after the deposition of the buffer layer. In the blend, the highest-occupied molecular orbital (HOMO) energy level of the PVK polymer matches better with the HOMO energy level of the emissive material (the HOMO level of both is −5.8 ev); therefore, the transfer of the holes may be facilitated across the interface by deposition of the buffer layer. This phenomenon can be observed in the reduction of the turn-on voltage and the increase in the efficiency of devices with the buffer layer.

Nonetheless, the morphological treatment of the interface cannot be the only reason for the improvement in device properties because both the metal and the dielectric ultrathin layers introduce similar morphological effects. As mentioned, the insertion of the metal ultrathin buffer layer leads to the accumulation of the current carriers at the interface, which has superb beneficial effects on the device performance. Notably, the accumulation of the current carriers forces the exciton formation zone to be displaced toward the interior part of the emissive layer, as compared schematically in Figure 4(a,b). Therefore, the exciton annihilation due to the collision at the organic/organic interface is effectively suppressed, and the device presents enhanced performance. The mentioned redistribution of the exciton formation profile and the recombination zone can be tracked in electroluminescence (EL) spectra as well. Figure 7 compares the normalized EL spectra for the device without any buffer layer and the device with a Ag buffer layer. As can be seen, the spectrum is red-shifted due to the displacement of the recombination profile and also amplification of the microcavity effect because of the presence of the metal layer close to the recombination zone. Table I summarizes the property improvement for the fabricated devices as the buffer layer is employed.

Finally, to examine further and to confirm the role of the buffer layer in device performance, other devices with similar structure were fabricated, namely, device D, for which the thickness of the Ag buffer layer is changed to 2 nm, and devices E and F, in which aluminum is employed as the cathode electrode. As can be observed, in device F, the turn-on voltage was decreased and power efficiency was increased (as a result of adding the buffer layer) in comparison with device E. Consequently, similar performance improvement is achieved when an ultrathin metal buffer layer is introduced in the device structure with an aluminum cathode.

CONCLUSIONS

In conclusion, an ultrathin metal buffer layer has been inserted at the organic/organic interface to enhance performance in OLEDs. The organic/organic interface plays a crucial role in the device performance as, generally, the mobility of the holes exceeds the mobility of electrons in organic materials, and therefore the recombination zone takes place at or near the HTL/EML interface. By utilization of an appropriate buffer layer at the interface, exciton formation and exciton annihilation can be managed effectively. We observed that a metal buffer layer, Ag, can enhance the device efficiency, whereas a dielectric buffer

Table I. Properties of the Organic Light-Emitting Diodes

Device name	Buffer layer	Turn-on voltage (V)	Maximum current efficiency (cd/A)	Maximum power efficiency (lm/w)
A	none	11	1.5	0.3
B	MgF_2 (1 nm)	10	1.4	0.3
C	Ag (1 nm)	7	5.2	1.6
D	Ag (2 nm)	9	6.0	1.9
E[a]	none	9	10.2	2.8
F[a]	Ag (1 nm)	6	11.5	3.1

[a] Device with aluminum cathode electrode.

layer, MgF_2, does not affect the device performance noticeably. The experimental results show that the electrical properties of the device remain unchanged while the optical properties improve remarkably: the turn-on voltage reduces about 3 V, the current efficiency increases from ~1.5 cd/A to more than 5 cd/A, and the power efficiency increases from ~0.3 lm/W to more than 1.5 lm/W. The study of the morphology of the surface at the interface shows that distinguishable segregation of the blend components occurs at the surface; that is, the polymer part (PVK) of the blend remains at the surface. This phase segregation partially facilitates hole transport to the emissive layer. Nonetheless, the device performance enhancement is mainly associated with the accumulation of current carriers and consequently the redistribution of the recombination zone from near the interface toward the interior part of the emissive layer.

REFERENCES

1. Liu, F.; Nunzi, J.-M. *Appl. Phys. Lett.* **2011**, *99*, 123302.
2. Janghouri, M.; Mohajerani, E.; Amini, M. M.; Najafi, E.; Hosseini, H. *J. Electron. Mater.* **2013**, *42*, 10.
3. Shrotriya, V.; Yang, Y. *J. Appl. Phys.* **2005**, *97*, 054504.
4. Jabbour, G. E.; Kippelen, B.; Armstrong, N. R.; Peyghambarian, N. *Appl. Phys. Lett.* **1998**, *73*, 1185.
5. Janghouri, M.; Mohajerani, E.; Amini, M. M.; Najafi, E. *J. Lumin.* **2014**, *154*, 465.
6. Hung, L. S.; Tang, C. W.; Mason, M. G. *Appl. Phys. Lett.* **1997**, *70*, 152.
7. Nguyen, T. D.; Ehrenfreund, E.; Valy Vardeny, Z. *Science* **2012**, *337* (6091), 204.
8. Sun, Z.; Ding, X.; Ding, B.; Gao, X.; Hu, Y.; Chen, X.; He, Y.; Hou, X. *Org. Electron.* **2013**, *14*, 511.
9. Jang, H. J.; Park, C. Y.; An, J. S.; Lee, J. H.; Choi, B. H.; Oh, S. Y.; Lee, C. H. *Org. Electron.* **2015**, *24*, 51.
10. Lin, H.; Yu, J.; Zhang, W. *Optoelectron. Lett.* **2012**, *8*, 197.
11. Li, F.; Tang, H.; Anderegg, J.; Shinar, J. *Appl. Phys. Lett.* **1997**, *70*, 1233.
12. Kang, S. J.; Park, D. S.; Kim, S. Y.; Whang, C. N.; Jeong, K.; Im, S. *Appl. Phys. Lett.* **2002**, *81*, 2581.
13. Brabec, C. J.; Shaheen, S. E.; Winder, C.; Sariciftci, N. S. *Appl. Phys. Lett.* **2002**, *80*, 7.
14. Jabbour, G. E.; Wang, J. F.; Peyghambarian, N. *Appl. Phys. Lett.* **2002**, *80*, 11.
15. Chen, B. J.; Sun, X. W. *Semicond. Sci. Tech.* **2005**, *20*, 801.
16. Kalhor, D.; Mohajerani, E.; HashemiPour, O. *J. Lumin.* **2015**, *167*, 376.
17. Bussac, M.; Michoud, D.; Zuppiroli, L. *Phys. Rev. Lett.* **1998**, *81*, 1678.
18. Arkhipov, V. I.; Emelianova, E. V.; Tak, Y. H.; Bässler, H. *J. Appl. Phys.* **1998**, *84*, 848.
19. Masenelli, B.; Berner, D.; Bussac, M. N.; Nüesch, F.; Zuppiroli, L. *Appl. Phys. Lett.* **2001**, *79*, 4438.
20. Scott, J. C. *J. Vac. Sci. Technol. A* **2003**, *21*, 521.
21. Fathollahi, M.-R.; Boroumand, F. A.; Raissi, F.; Sharifi, M.-J. *Org. Electron.* **2012**, *13*, 905.
22. Gozzi, G.; Queiroz, E. L.; Zucolotto, V.; Faria, R. M.; Chinaglia, D. L. *Phys. Status Solidi B* **2015**, *252*, 404.
23. Fathollahi, M.-R.; Sharifi, M.-J.; Boroumand, F. A.; Raissi, F.; Mohajerani, E. *J. Photon. Energy* **2015**, *5*, 057610.
24. Janghouri, M.; Mohajerani, E.; Amini, M. M.; Najafi, E. *Appl. Phys. A* **2014**, *114*, 445.